Journal of Solid State Chemistry 183 (2010) 392–401

Contents lists available at ScienceDirect

Journal of Solid State Chemistry

journal homepage: www.elsevier.com/locate/jssc

Neutron diffraction study of the crystal structure and structural phase transition of $La_{0.7}Ca_{0.3-x}Sr_xCrO_3$ ($0 \le x \le 0.3$) The relationship between thermodynamic behavior and crystal structure changes at the phase transition

Kazuki Omoto [a], Stefan T. Norberg [b,c], Steve Hull [c], Akimitsu Aoto [a], Takuya Hashimoto [a,*]

[a] Department of Integrated Sciences in Physics and Biology, College of Humanities and Sciences, Nihon University, 3-25-40 Sakurajousui, Setagaya-ku, Tokyo 156-8550, Japan
[b] Department of Chemical and Biological Engineering, Chalmers University of Technology, SE-412 96 Gothenburg, Sweden
[c] The ISIS Facility, Rutherford Appleton Laboratory, Chilton, Didcot, OX11 0QX, UK

ARTICLE INFO

Article history:
Received 16 September 2009
Received in revised form
21 November 2009
Accepted 29 November 2009
Available online 5 December 2009

Keywords:
$La_{0.7}Ca_{0.3-x}$ Sr_xCrO_3
Interconnector
Solid oxide fuel cells
Structural phase transition
Neutron diffraction
Rietveld refinement

ABSTRACT

The crystal structure of the $La_{0.7}Ca_{0.3-x}Sr_xCrO_3$ series, including the compositional and temperature dependence of the structural parameters, has been studied by variable temperature neutron diffraction measurements. The extent of the distortions from the ideal cubic perovskite structure has been evaluated quantitatively using the average bond lengths and the mean volumes of the [CrO_6] octahedron and [(La/Ca/Sr)O_{12}] polyhedron, and has been shown to decrease with increase of Sr content or temperature. At the structural phase transition from the orthorhombic (*Pnma*) structure to the rhombohedral ($R\bar{3}c$) one, the volume of the [CrO_6] octahedron decreases whereas that of the [(La/Ca/Sr)O_{12}] polyhedron shows little difference, resulting in an overall decrease in the level of distortion. The change in the degree of distortion at the phase transition decreases with increase of Sr content, in agreement with the smaller variation of the enthalpy and volume for the specimens with higher Sr content.

1. Introduction

Electronically conducting oxides have been extensively examined at high temperatures for technological applications within various energy generation devices. One of the most promising energy conversion technologies is the solid oxide fuel cell (SOFC), which possesses very high energy conversion efficiency. In order to generate high voltages from an SOFC it is necessary to employ an interconnector to connect individual SOFCs in series. The material chosen for the interconnector must be stable at the typical SOFC operating temperature (1000–1300 K) under both oxidizing and reducing gas atmospheres. In this context, compounds in the series $La_{1-x}A_xCrO_3$ (A=Ca, Sr) have been investigated, since they possess a high electrical conductivity and high chemical stability at elevated temperatures under reductive atmospheres [1]. However, several problems have been raised for the application of $La_{1-x}A_xCrO_3$, including its poor sinterability. It was reported that partial Sr substitution onto the La site improves the sintering properties, though it has proved difficult to obtain specimens with high enough sintering density for applications as an interconnector [2]. It has also been reported that partial Ca substitution or the addition of excess Ca is an effective approach to improve the sintering properties [2–5], with liquid phase sintering resulting in the preparation of specimens with sintering densities of over 95% synthesized by the addition of excess Ca. However, an additional serious problem is the presence of a structural phase transition between room temperature and the SOFC operating temperatures, which remains in the Ca substituted $LaCrO_3$ system.

At room temperature, the crystal structure of $LaCrO_3$ can be described as an orthorhombic distortion of the cubic perovskite structure in space group *Pnma* (no. 62). At 533 K a structural phase transition to a rhombohedrally distorted perovskite with space group $R\bar{3}c$ (no. 167) is observed [6–10]. Fig. 1 shows a schematic drawing of (a1) the orthorhombic distorted perovskite and (b1) the rhombohedrally distorted one, prepared with program VENUS [11]. The tilt and rotation of the [CrO_6] octahedron can be described as $a^+b^-b^-$ and $a^-a^-a^-$ for orthorhombic phase and rhombohedral one, respectively, by using Glazer notation [12,13]. The relationship between the ideal cubic perovskite unit cell and (a2) the orthorhombic distorted one and (b2) the rhombohedrally distorted one are

* Corresponding author. Fax: +81 3 5317 9432.
E-mail address: takuya@chs.nihon-u.ac.jp (T. Hashimoto).

0022-4596/$ - see front matter © 2009 Elsevier Inc. All rights reserved.
doi:10.1016/j.jssc.2009.11.028

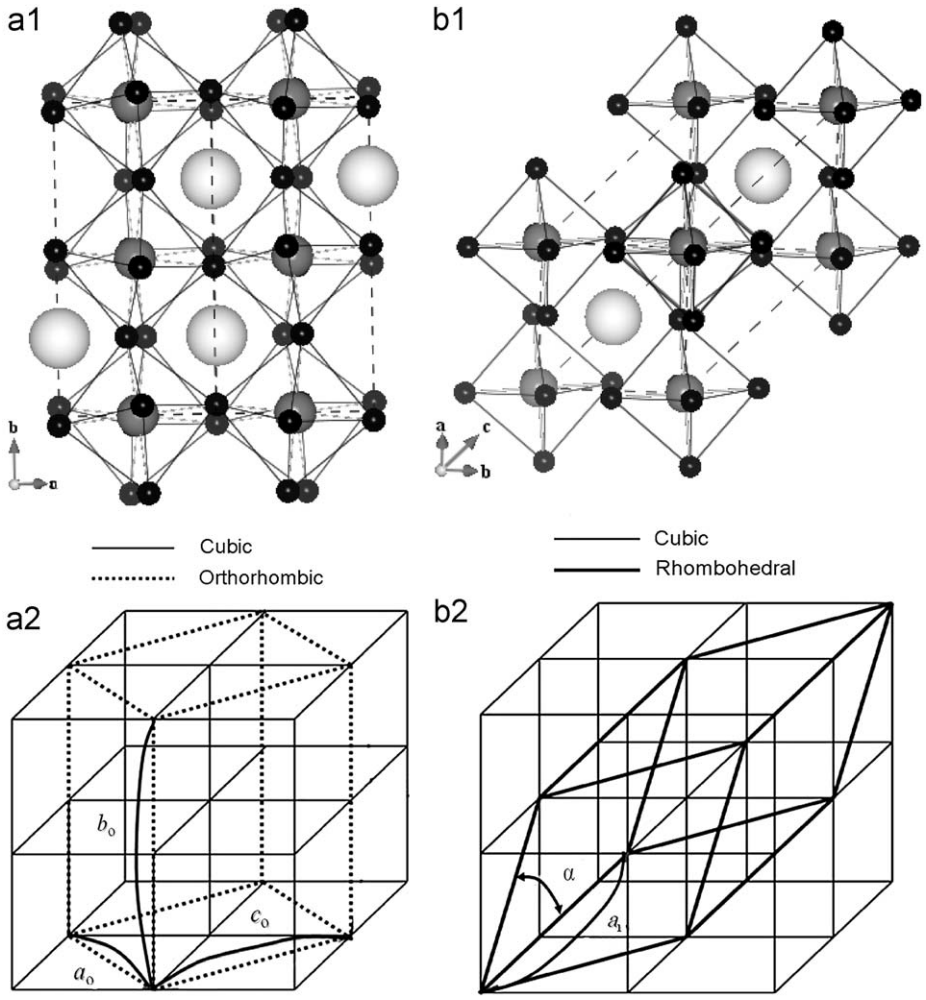

Fig. 1. Crystal structure drawing of (a1) the orthorhombic distorted perovskite (space group: *Pnma*) and (b1) the rhombohedrally distorted one (space group: $R\bar{3}c$) prepared with program VENUS [11]. Small black sphere and large white one represent O^{2-} and $La^{3+}/Ca^{2+}/Sr^{2+}$, respectively. Cr ion is shown as light black sphere. The relationship between the ideal cubic perovskite unit cell and (a2) the orthorhombic distorted perovskite unit cell and (b2) the rhombohedrally distorted one is also shown. For an ideal cubic perovskite structure, $a/\sqrt{2}$, $b/2$ and $c/\sqrt{2}$ of the orthorhombic lattice are the same and α the angle of the rhombohedrally distorted phase is equal to 60°.

also depicted in Fig. 1. As this is a first order phase transition, it is accompanied by latent heat and discrete change in the volume, resulting in deterioration of the mechanical toughness and reliability of the SOFC [4]. Thus, for applications of $LaCrO_3$ based compounds as interconnectors within an SOFC, no structural phase transition should occur between room temperature and the SOFC operating temperature. However, the phase transition temperature in $La_{1-x}Ca_xCrO_3$ is observed to increase with increase of the Ca content [14,15]. Conversely, the phase transition temperature decreases with increase of Sr content in $La_{1-x}Sr_xCrO_3$, resulting in materials free from the phase transition over the temperature range of interest for x larger than 0.10 [16–18]. As a consequence, it might be expected that ceramic specimens possessing good sintering properties and an absence of the phase transition might be prepared by simultaneous substitution of Ca and Sr onto the La site.

In our preceding papers [19,20], excellent sintering properties of $La_{0.70}Ca_{0.3-x}Sr_xCrO_3$ ceramic specimens were reported, with a sintering density in excess of 93% for specimens with x=0.10–0.25. In addition, the phase transition temperature was observed to decrease with increase of the Sr content, resulting in an absence of the phase transition between room temperature and SOFC operating temperature for x larger than 0.20. Furthermore, differential scanning calorimetry (DSC), dilatometry and variable temperature X-ray diffraction studies indicated that the variation of the enthalpy and volume at the phase transition, ΔH and ΔV, decrease with increase of Sr content. However, the origin of the decreases in the phase transition temperature, ΔH and ΔV, which can be regarded as important information for the control of the phase transition behavior, has not been clarified.

It might be expected that the variation of the phase transition behavior is related to changes in the crystal structure with temperature and substitution, including variations in the volume of the [CrO_6] octahedra, tilt angle, Cr–O–Cr angle and so on. Since the positions and thermal parameters of the oxide ions within metal oxides cannot be evaluated accurately using powder X-ray diffraction, such information was not presented in our previous paper [20]. However, whilst we could not clarify the origin of the smaller ΔH and ΔV with increase of Sr content, it was speculated that the variation of the distortion from the ideal cubic perovskite arrangement inferred from variations of the lattice parameters might be related to the variation of ΔH and ΔV. Subtle changes in the crystal structure can be more accurately evaluated using neutron diffraction, especially in the case of the positional and thermal parameters of the oxide ions. However, there have been few reports of neutron diffraction measurements of $LaCrO_3$ based compounds. Sakai and co-workers reported the temperature variation of the crystal structure of the $La_{1-x}Ca_xCrO_3$ system using neutron diffraction and observed an increase of the phase transition temperature and decrease of ΔV with increase of Ca

content [21]. Nevertheless, the origin of the variation of the phase transition behavior was not discussed. Oikawa and co-workers carried out a variable temperature neutron diffraction study of the $LaCrO_3$ system [22] and clarified the decrease of the distortion from the ideal cubic perovskite structure and shrinkage of the [CrO_6] octahedra at the phase transition. Since their measurements were limited to the parent $LaCrO_3$ compound, the origin of the variation of the phase transition behavior with Sr or Ca substitution was not addressed.

In this study, the crystal structure of $La_{0.7}Ca_{0.3-x}Sr_xCrO_3$ and its variation with composition and temperature have been investigated using variable temperature neutron powder diffraction. The origin of the decrease of ΔH and ΔV with Sr content has been proposed from the analysis of the structural behavior at the phase transition.

2. Experimental

2.1. Sample preparation

The ceramic $La_{0.7}Ca_{0.3-x}Sr_xCrO_3$ specimens were prepared by Pechini method [23] using powdered La_2O_3, $SrCO_3$, $CaCO_3$, (99.9%, Furuuchi Chemical Co., Ltd.) and $Cr(NO_3)_3 \cdot 9H_2O$ (99.9%, Wako Chemical Co., Ltd.), from which the specimens with correct chemical composition were prepared. Prior to preparation, the La_2O_3 was heated in air at 1473 K for 12 h to decompose impurities such as $La(OH)_3$ and $La_2(CO_3)_3$. $SrCO_3$ and $CaCO_3$ were dried at 393 K for 6 h in air. The H_2O content in the $Cr(NO_3)_3 \cdot 9H_2O$ was confirmed by thermogravimetric measurement. Raw materials in the stoichiometric ratio were completely dissolved in diluted nitric acid before excess citric acid was added to the solution to obtain the chelate of each metal. After the addition of excess ethylene glycol, the solution was heated at about 570 K and the solution changed to a polyester resin, which was burned to powder. The resultant powder was calcined at 1023 K for 7 h in air, followed by crushing using a planet-type ball mill (LBP-MINI: Itoh Seisakusho Co., Ltd.) employing yttria-stabilized ZrO_2 as the material for both pot and ball (manufactured by Nikkato Corp.) in air at 250 rpm for 1 h. The resultant powder was uniaxially pressed into pellets at a pressure of 100 MPa, sintered at 1673 K for 17 h in air and then crushed into powder using an Al_2O_3 mortar. The crystal structures of the samples were checked by Cu$K\alpha$ X-ray diffraction measurements (50 kV, 250 mA, RINT-2500; Rigaku Co., Ltd.) at room temperature, which revealed that the samples with x less than 0.15 and more than 0.20 possess the orthorhombic and rhombohedral distortions of the perovskite structure, respectively, in agreement with the previous reports [19,20].

2.2. Variable temperature neutron diffraction measurements

Neutron diffraction measurements employing the time of flight technique were performed using the POLARIS powder diffractometer at the ISIS facility, Rutherford Appleton Laboratory, UK [24], using the backscattering detector bank (covering scattering angles of $130^\circ < 2\theta < 160^\circ$, giving a d-spacing range of $0.2 < d(\text{Å}) < 3.2$, with a resolution of $\Delta d/d \sim 5 \times 10^{-3}$), the 90° bank ($85^\circ < 2\theta < 95^\circ$, $0.3 < d(\text{Å}) < 4.1$, $\Delta d/d \sim 7 \times 10^{-3}$), and the low angle bank ($28^\circ < 2\theta < 42^\circ$, $0.5 < d(\text{Å}) < 8.3$, $\Delta d/d \sim 10^{-2}$). All powder samples were encapsulated in cylindrical vanadium cans, and the series of $La_{0.7}Ca_{0.3-x}Sr_xCrO_3$ compounds with x=0.00, 0.05, 0.10, 0.15, 0.20, 0.25, and 0.30 were initially measured at room temperature. Variable temperature scans were subsequently performed on $La_{0.7}Sr_{0.3}CrO_3$ (from 4.2(2) to 300(2) K, in steps of 20 K), $La_{0.7}Ca_{0.15}Sr_{0.15}CrO_3$ (from 4.2(2) to 773(3) K in steps of 20 K), and $La_{0.7}Ca_{0.3}CrO_3$ (from 473(2) to 973(3) K, in steps of 20 K). $La_{0.7}Ca_{0.15}Sr_{0.15}CrO_3$ was chosen from amongst the $La_{0.7}Ca_{0.3-x}Sr_xCrO_3$ compositions for detailed study because it shows the most impressive sintering properties [20]. The low temperature measurements were performed using a standard helium cooled cryostat, whilst the high temperature measurements employed a furnace constructed of vanadium foil resistive heater elements and heat shields.

2.3. Analysis of crystal structure and its temperature dependence

Rietveld refinements of the neutron powder diffraction data were carried out using the program GSAS [25] and the structural parameters, bond lengths and bond angles were evaluated using the program VENUS [11]. The volumes of the [(La/Ca/Sr)O_{12}] polyhedron, V_A, the [CrO_6] octahedron, V_B and their ratio V_A/V_B were evaluated using the formula derived by Thomas and co-workers [26–28] and previously used in the study of undoped $LaCrO_3$ [22]. The parameter, Φ, which has been frequently employed to estimate the degree of tilt from the ideal cubic perovskite structure [22,26–28], was also calculated using the expression,

$$\Phi = \frac{1}{6}\left(5 - \frac{V_A}{V_B}\right)$$

3. Results and discussion

Fig. 2 shows two typical examples of the Rietveld refinements, using the neutron powder diffraction data collected from $La_{0.7}Ca_{0.15}Sr_{0.15}CrO_3$ at (a) 300 K and (b) 473 K. The structural parameters obtained are listed in Table 1, with the typical R_w values of ~3% indicating successful Rietveld refinement. Fits of comparable quality were obtained for all samples and at all the measurement temperatures.

3.1. Structural variation of $La_{0.7}Ca_{0.3-x}Sr_xCrO_3$ with x at room temperature

Fig. 3 shows the unit cell volumes and lattice parameters of $La_{0.7}Ca_{0.3-x}Sr_xCrO_3$ at room temperature determined by Rietveld refinement of the neutron powder diffraction data. The crystal structures of the specimens with x less than 0.15 and more than 0.20 were confirmed to be the orthorhombic and rhombohedral distorted perovskite arrangements, respectively. An increase in the unit cell volume with increase of x was observed, indicating that Sr can be successfully substituted onto the La site. The difference between the $a/\sqrt{2}$, $b/2$ and $c/\sqrt{2}$ values increases with increase of Sr content in the orthorhombic phase whilst the rhombohedral angle, α, decreases and approaches 60° in the rhombohedral phase, suggesting a greater and lesser distortion in the orthorhombic and rhombohedral phases, respectively, within samples with a high Sr content, as Fig. 1(a2) and (b2) depict. These trends were also confirmed by X-ray diffraction measurements reported in the previous studies [20]. However, this suggestion contradicts that expected on the basis of the tolerance factor of $La_{0.7}Ca_{0.3-x}Sr_xCrO_3$ calculated from the ionic radii proposed by Shannon [29], which approaches unity with increased Sr content. Consequently, a more detailed analysis of the structural behavior, including the bond lengths, V_A and V_B, is required to allow a discussion of the extent of distortion from the ideal cubic perovskite structure.

Fig. 4(a) shows the variation of the average bond length of Cr–O (represented as $\overline{Cr-O}$) and (La/Sr/Ca)–O (represented as $\overline{La-O}$)

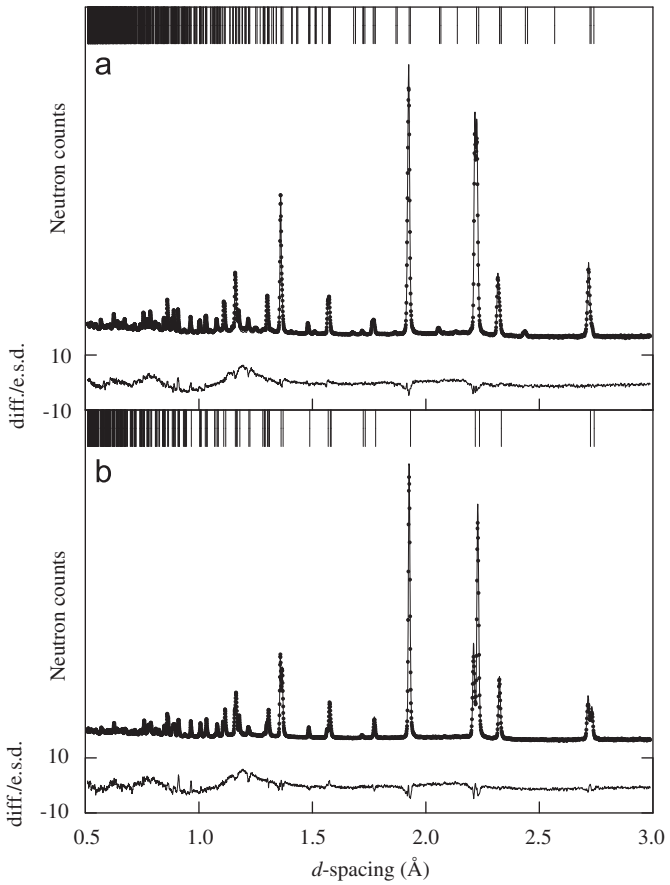

Fig. 2. Representative Rietveld refinement patterns of $La_{0.7}Ca_{0.15}Sr_{0.15}CrO_3$ at (a) 290(2) K and (b) 473(2) K. The dots are the experimental data points and the solid line is the calculated profile using the parameters listed in Table 1. The lower trace shows the difference (measured minus calculated) divided by the estimated standard deviation on the experimental data points. The row of tick marks along the top of the figure denotes the calculated positions of all the symmetry allowed Bragg reflections.

Table 1
Summary of the results of the least-squares refinements of the neutron diffraction data collected from $La_{0.7}Ca_{0.15}Sr_{0.15}CrO_3$ at 290(2) and 473(2) K.

Temperature	290(2) K	473(2) K
Phase	orthorhombic	rhombohedral
Space group	*Pnma*	$R\bar{3}c$
Lattice parameters	a=5.44603(14)Å	a=5.48357(6)Å
	b=7.7047(2)Å	c=13.3070(3)Å
	c=5.48029(15)Å	
Unit cell volume	V=229.952(11)Å^3	V=346.527(9)Å^3
La/Ca/Sr	4(*c*) at *x*,1/4, *z*, *etc.*	6(*a*) at 0,0,1/4, *etc.*
	x=0.0115(4)	
	z=−0.0018(4)	
	u=0.0043(2)Å^2	u=0.0069(2)Å^2
Cr	4(*b*) at 0,0,1/2, *etc.*	6(*b*) at 0,0,0, *etc.*
	u=0.0024(2)Å^2	u=0.0045(3)Å^2
O1	4(*c*) at *x*,1/4,*z*, *etc.*	18(*e*) at *x*,0,1/4, *etc.*
	x=0.4957(6)	x=0.54688(10)
	z=−0.0580(4)	
	u=0.0059(3)Å^2	u=0.0108(2)Å^2
O2	8(*d*) at *x*,*y*,*z*, etc.	–
	x=0.2324(3)	
	y=0.5295(2)	
	z=−0.2330(3)	
	u=0.0063(2)Å^2	
Weighted profile *R*-factor	0.0369	0.0332
Expected *R*-factor	0.0084	0.0084
Number of data points	4502	4502
Number of fitted parameters	28	17
Reduced χ^2	19.30	15.62

The weighted profile and expected *R*-factors are given by

$$R_{wp}^2 = \sum_{N_d} \frac{(y_{obs}\text{-}y_{calc})^2}{(\sigma y_{obs})^2} \Big/ \sum_{N_d} \frac{(y_{obs})^2}{(\sigma y_{obs})^2} \quad \text{and} \quad R_{exp}^2 = (N_d\text{-}N_v) \Big/ \sum_{i=1}^{N_d} \frac{(y_{obs})^2}{(\sigma y_{obs})^2},$$

respectively and the summations are made over the N_d data points used in the fit. N_v is the number of fitted variables. y_{obs} and y_{calc} are the observed and calculated intensities, respectively, and σy_{obs} is the estimated standard deviation on y_{obs} derived from the counting statistics. The reduced χ^2 value is given by $\chi^2 = R_{wp}^2/R_{exp}^2$.

at room temperature obtained in this study. $\overline{Cr-O}$ decreases and $\overline{La-O}$ increases with increase of the Sr content, with a discontinuity observed at around x=0.15–0.20 due to the change in the crystal structure. As an approximate but simple evaluation of the degree of distortion from the ideal cubic perovskite structure, the parameter

$$t = \frac{1}{\sqrt{2}} \frac{\overline{La-O}}{\overline{Cr-O}}$$

was calculated and is shown in Fig. 4(b). In the case of the ideal cubic perovskite structure, t equals 1. Although t=1 does not necessarily mean that ideal cubic perovskite is observed (since averaged polyhedra are assumed), we regard this parameter as useful to estimate the degree of distortion. It is observed that, whilst an abrupt increase due to the structural phase transition occurs at around x=0.15–0.20, t linearly approaches 1 with increasing Sr content in both phases. This suggests that the level of structural distortion becomes smaller with higher Sr content in both the orthorhombic and rhombohedral phases. In a previous paper, we speculated from the variation of the lattice constants with Sr content that the Gibbs formation energy of $La_{1-x-y}Ca_xSr_yCrO_3$ would decrease with decreasing distortion and that the decrease of phase transition temperature, ΔH and ΔV with Sr content could be attributed to the increase and decease of the distortion in the orthorhombic and rhombohedral phases, respectively [20]. Fig. 4 indicates that this speculation needs to be corrected.

In order to estimate the degree of distortion more precisely, the parameter Φ was calculated. We regard that, though not decisive, Φ is preferential to the t parameter, because it is based on unaveraged polyhedra and has been generally employed for estimation of distortion of various perovskite materials [26–28]. Fig. 5 shows the variation of V_A and V_B with Sr content. The ratio V_A/V_B is also presented in Fig. 5. An increase of V_A and decrease of V_B with increasing Sr content is observed, so that the value of V_A/V_B increases and approaches a value of around 5. The parameter Φ is calculated from the V_A/V_B values and shown on the right hand side of the vertical axis. Since Φ is equal to zero for a sample possessing the ideal cubic perovskite structure [22,26–28], the observed behavior of Φ shows agreement with the finding of a lower distortion for the specimens with high Sr content. At around x=0.15–0.20, a discontinuity due to the structural phase transition is seen, especially in the case of V_B, resulting in an abrupt increase in V_A/V_B and decrease in Φ. Since the decrease of V_B has also been observed in the structural phase transition of $LaCrO_3$ as a function of temperature [22], it can be supposed that the behavior of the structural phase transition due to changing the cation composition in $La_{0.7}Sr_{0.3-x}Ca_xCrO_3$ is similar to that caused by temperature. To confirm this hypothesis and address the issue of the thermodynamic behavior of the structural phase transition, the variation of the crystal structure of $La_{0.7}Sr_{0.3-x}Ca_xCrO_3$ with temperature was investigated.

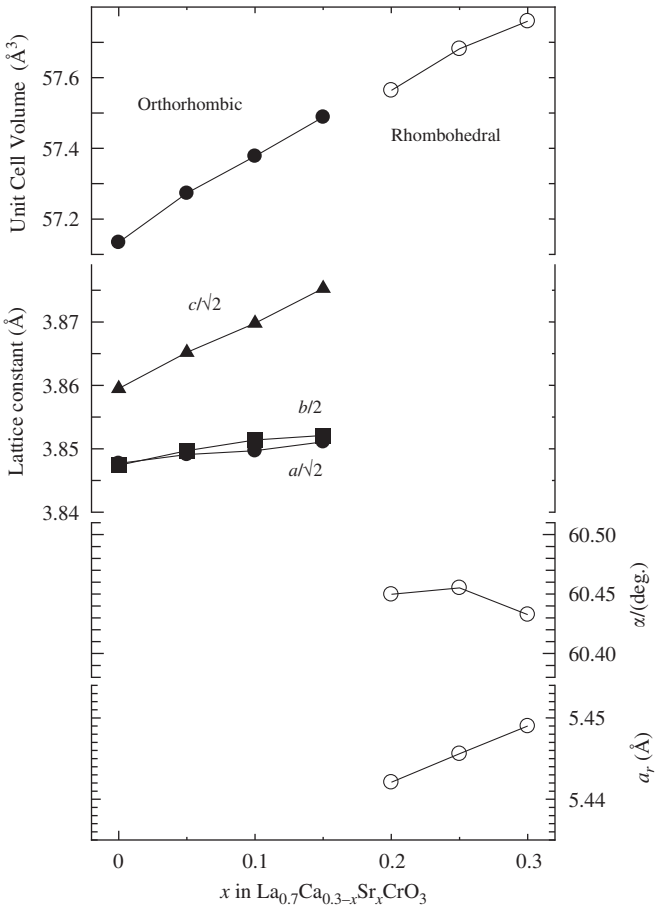

Fig. 3. Unit cell volumes and lattice parameters of $La_{0.7}Ca_{0.3-x}Sr_xCrO_3$ at room temperature determined by Rietveld refinement of the neutron powder diffraction data. The closed and open symbols represent data refined using the orthorhombic and rhombohedral structural models, respectively.

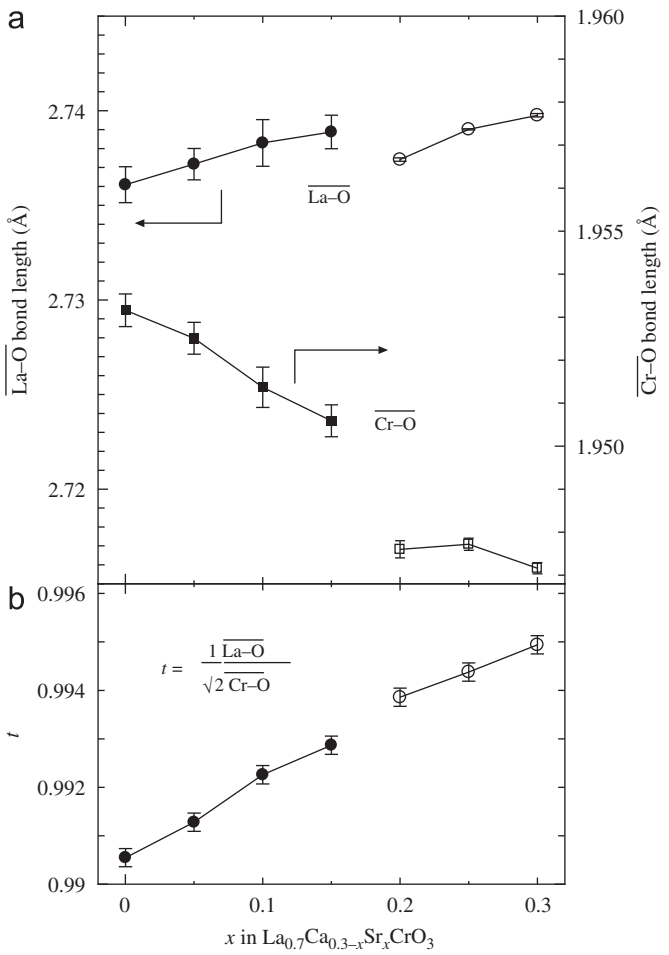

Fig. 4. (a) Average bond lengths of Cr–O and La–O and (b) parameter, t, calculated using $t = \overline{La–O}/(\sqrt{2}\,\overline{Cr–O})$, in $La_{0.7}Ca_{0.3-x}Sr_xCrO_3$ at room temperature.

3.2. Temperature variation of lattice constants and distortion of $La_{0.7}Sr_{0.3}CrO_3$

High temperature X-ray diffraction and thermal analyses, such as dilatometry and DSC, revealed that no structural phase transition occurs in $La_{0.7}Sr_{0.3}CrO_3$ from room temperature to 1273 K [17]. In this work, the crystal structure of $La_{0.7}Sr_{0.3}CrO_3$ was studied from 4.2 to 300 K and all the diffraction patterns could be refined using the rhombohedrally distorted perovskite structural model.

Fig. 6 shows the temperature dependence of the lattice parameters and unit cell volume of $La_{0.7}Sr_{0.3}CrO_3$. In the temperature range from 4.2 to about 50 K, the changes of the a-axis, α and the unit cell volume are approximately equal to zero. This indicates that the third law of thermodynamics can be applied in this temperature range. In addition, as shown in Fig. S1, the positional parameter of the oxide ion (description of hexagonal lattice) is constant within this temperature range. At temperatures greater than around 50 K, the a-axis and volume increase, plus that α approaches 60°, suggesting a lower distortion at the highest temperatures. The positional parameter of the oxide ion also changes. The thermal parameters of all the ions increase with increasing temperature, as depicted in Fig. S2 that indicating chemical bonding becomes softer with increase of temperature.

In order to evaluate the variation of the crystal structure with temperature more minutely, the average bond lengths and the volumes V_A and V_B were calculated. A decrease in the extent of the structural distortion at high temperature is supported by the variation of $\overline{La–O}$, $\overline{Cr–O}$ and t illustrated in Fig. 7. The parameter t approaches 1 with increase of temperature. Finally, Fig. 8 shows the temperature dependence of V_A, V_B, V_A/V_B and Φ. Φ approaches zero with increase of temperature, again consistent with a lower distortion at high temperature.

3.3. Temperature dependence of the crystal structure of $La_{0.7}Ca_{0.3}CrO_3$ and $La_{0.7}Ca_{0.15}Sr_{0.15}CrO_3$

The diffraction patterns of $La_{0.7}Ca_{0.3}CrO_3$ could be refined using the orthorhombic and rhombohedral perovskite structures below and above 725 K, respectively. This is consistent with the presence of a structural phase transition at 725 K determined by DSC [20]. Fig. 9 shows the temperature dependence of the lattice parameters and unit cell volume of $La_{0.7}Ca_{0.3}CrO_3$, with an almost linear thermal expansion observed in each case. The difference between $a/\sqrt{2}$, $b/2$ and $c/\sqrt{2}$ within the orthorhombic phase shows little variation with temperature, which is a different behavior to that observed on increase of Sr content in $La_{0.7}Ca_{1-x}Sr_xCrO_3$ at room temperature (see Fig. 3). At the phase transition, a small decrease in the unit cell volume was observed, as illustrated in the inset of Fig. 9, which was also detected by high-temperature X-ray diffraction and dilatometry measurements [19,20]. Fig. 10 shows the positional parameters evaluated by Rietveld refinement of the neutron powder diffraction patterns. The positional parameter, z, of the cations is almost constant, whilst those of x of the cation and the oxide ion

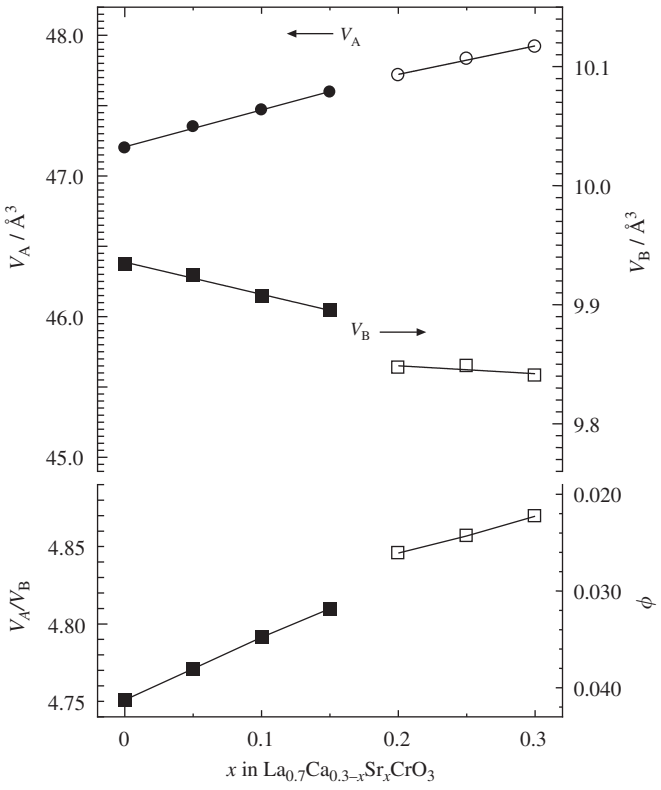

Fig. 5. Variation of V_A, V_B, V_A/V_B and Φ with Sr content in $La_{0.7}Ca_{0.3-x}Sr_xCrO_3$ at room temperature.

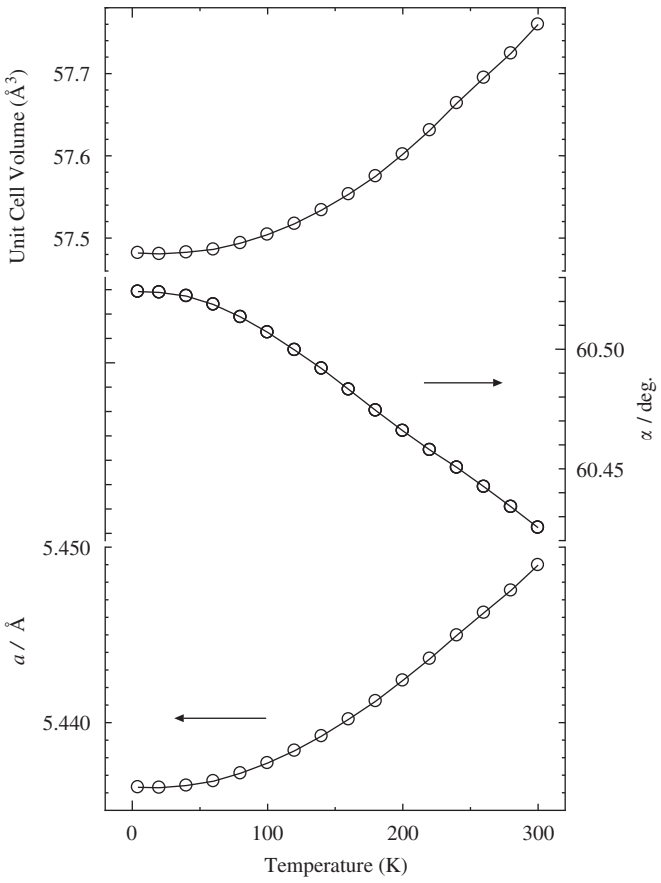

Fig. 6. Temperature dependence of the unit cell volume and lattice parameters of $La_{0.7}Sr_{0.3}CrO_3$.

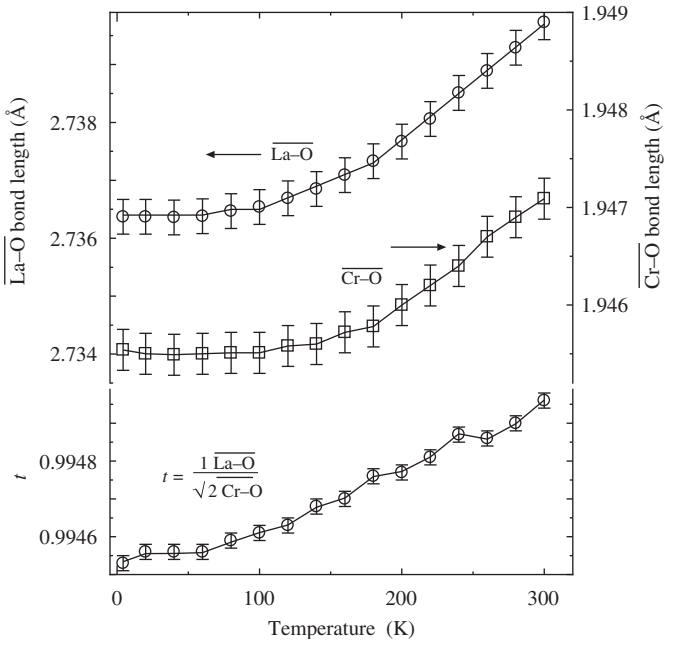

Fig. 7. Temperature dependence of the average bond length of La–O and Cr–O and parameter, t, of $La_{0.7}Sr_{0.3}CrO_3$.

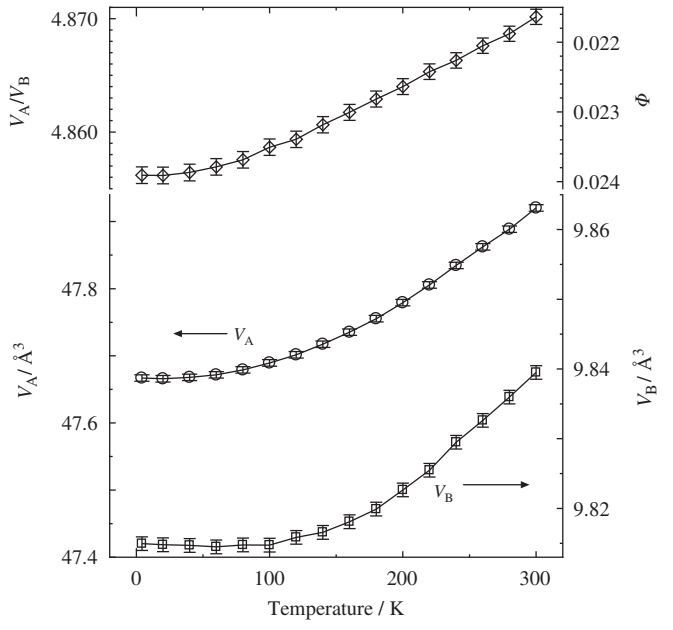

Fig. 8. Temperature dependence of V_A, V_B, V_A/V_B and Φ for $La_{0.7}Sr_{0.3}CrO_3$.

show significant temperature dependence. As illustrated in Fig. S3, all the thermal parameters increase with increase of temperature, showing softening of the chemical bond. The discontinuous variation due to the structural phase transition at around 725 K suggests that the structural phase transition involves a discrete change in the chemical bond strength.

In order to investigate the effect of simultaneous substitution of Sr and Ca, diffraction patterns of $La_{0.7}Ca_{0.15}Sr_{0.15}CrO_3$ were collected and refined as a function of temperature. Diffraction patterns below 353 K could be refined assuming the orthorhombic structure whilst those collected above 373 K required the use of the rhombohedral model. The observed phase transition temperature agreed well with that reported by DSC and dilatometry

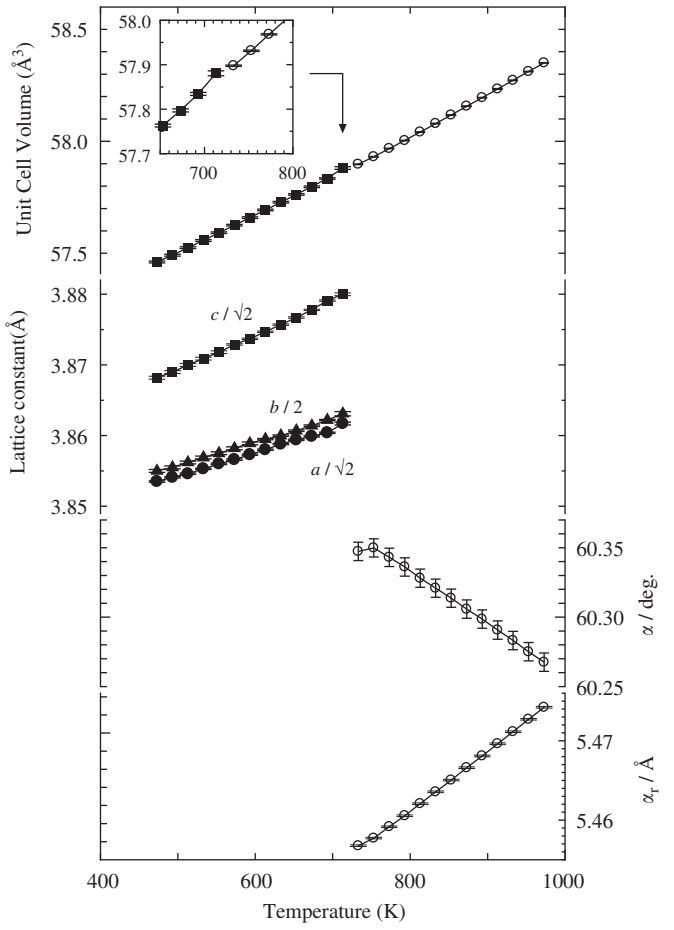

Fig. 9. Temperature dependence of the unit cell volume and lattice parameters of $La_{0.7}Ca_{0.3}CrO_3$. The closed and open symbols represent data refined using the orthorhombic and rhombohedral structural models, respectively. An expanded view of the temperature dependence of the unit cell volume around 725 K is shown in the inset.

[19,20]. Fig. 11 shows the temperature dependence of the lattice parameters and unit cell volume of $La_{0.7}Ca_{0.15}Sr_{0.15}CrO_3$, with almost constant lattice parameters observed over the temperature range from 4.2 to 100 K. At temperatures above around 100 K, an almost linear thermal expansion is observed for each lattice parameter, in both orthorhombic and rhombohedral phases. The differences between the $a/\sqrt{2}$, $b/2$ and $c/\sqrt{2}$ values in the orthorhombic phase show little change with temperature, which is the similar behavior to $La_{0.7}Ca_{0.3}CrO_3$. A decrease in the unit cell volume is observed at the orthorhombic to rhombohedral phase transition, although its size, ΔV, is smaller than that observed in $La_{0.7}Ca_{0.3}CrO_3$ (see inset in Fig. 11). The variation of the positional parameters with temperature is illustrated in Fig. 12 and, in the case of the oxide ions and parameter x of cation, shows similar temperature dependence to those for $La_{0.7}Ca_{0.3}CrO_3$ depicted in Fig. 10. Conversely, the cations' positional parameter, z, within the orthorhombic phase showed rather different behavior to those of $La_{0.7}Ca_{0.3}CrO_3$, gradually approaching zero with increase of temperature. The dependence of the thermal parameters with temperature is shown in Fig. S4. All the thermal parameters increased with increase of temperature within the same phase, suggesting softening of chemical bond. Discontinuous change at the phase transition temperature was observed which is similar to the case of $La_{0.7}Ca_{0.3}CrO_3$. However, the thermal parameter of Cr in $La_{0.7}Ca_{0.15}Sr_{0.15}CrO_3$ increased at the phase transition whereas that in $La_{0.7}Ca_{0.3}CrO_3$ decreased. The origin of this behavior could not be clarified in this study.

3.4. Changes in the crystal structure at the phase transition in $La_{0.7}Ca_{0.3}CrO_3$ and $La_{0.7}Ca_{0.15}Sr_{0.15}CrO_3$. Effects of Sr substitution on the thermodynamic behavior of the phase transition and interconnector applications within SOFCs

Fig. 13 shows the temperature dependence of $\overline{La-O}$, $\overline{Cr-O}$ and t for $La_{0.7}Ca_{0.3}CrO_3$. A linear relationship is observed for $\overline{La-O}$ and $\overline{Cr-O}$ in both phases and an abrupt decrease in $\overline{La-O}$ and $\overline{Cr-O}$ is

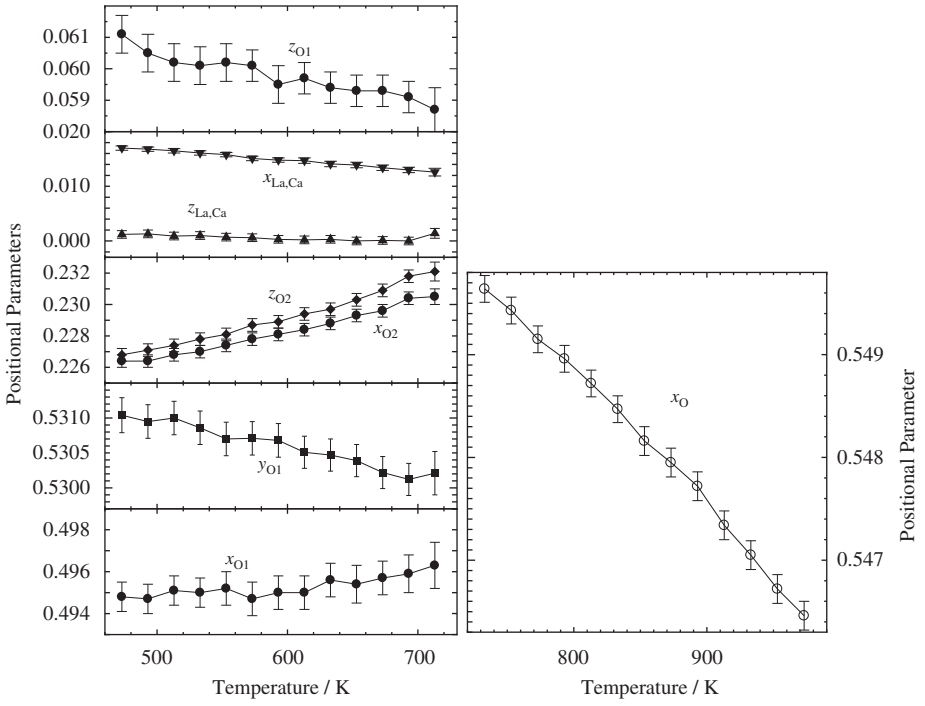

Fig. 10. Temperature dependence of the positional parameters of $La_{0.7}Ca_{0.3}CrO_3$.

observed at the phase transition. The parameter t approaches 1 with increasing temperature, indicating a lower distortion at higher temperature, and shows an abrupt increase at the phase transition. This tendency is the same as that observed in $LaCrO_3$ [21]. The variation of $\overline{La-O}$, $\overline{Cr-O}$ and t of $La_{0.7}Ca_{0.15}Sr_{0.15}CrO_3$ with temperature is shown in Fig. 14 and, apart from the temperature range below 100 K, its behavior is very similar to that of $La_{0.7}Ca_{0.3}CrO_3$ illustrated in Fig. 13.

In order to evaluate the distortion from the ideal cubic perovskite structure, V_A and V_B have been calculated and plotted as a function of temperature in Fig. 15. An almost linear relationship is obtained for the temperature dependence of V_A

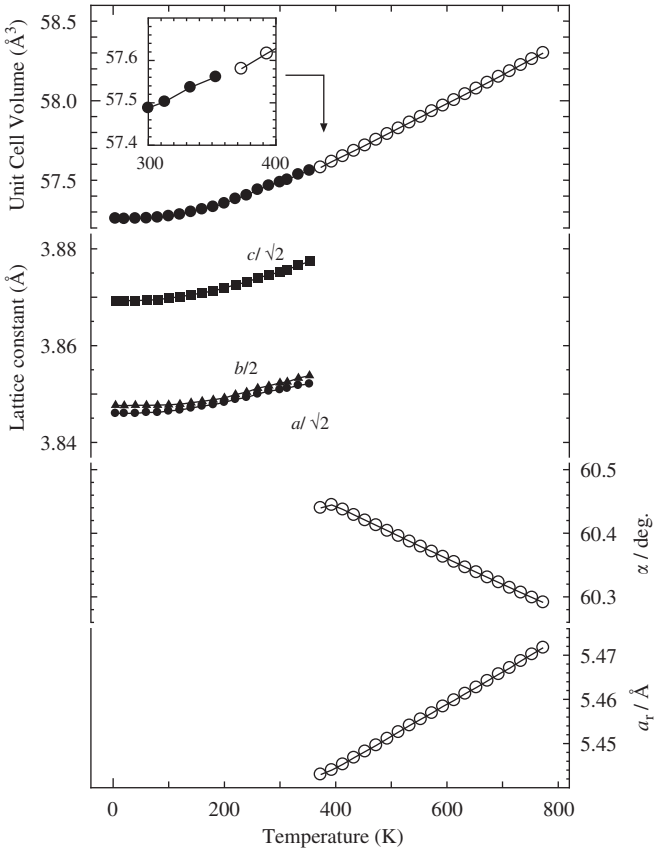

Fig. 11. Temperature dependence of the unit cell volume and lattice parameters of $La_{0.7}Ca_{0.15}Sr_{0.15}CrO_3$. The closed and open symbols represent data refined using the orthorhombic and rhombohedral structural models, respectively. An expanded view of the temperature dependence of the unit cell volume around 353 K is shown in the inset.

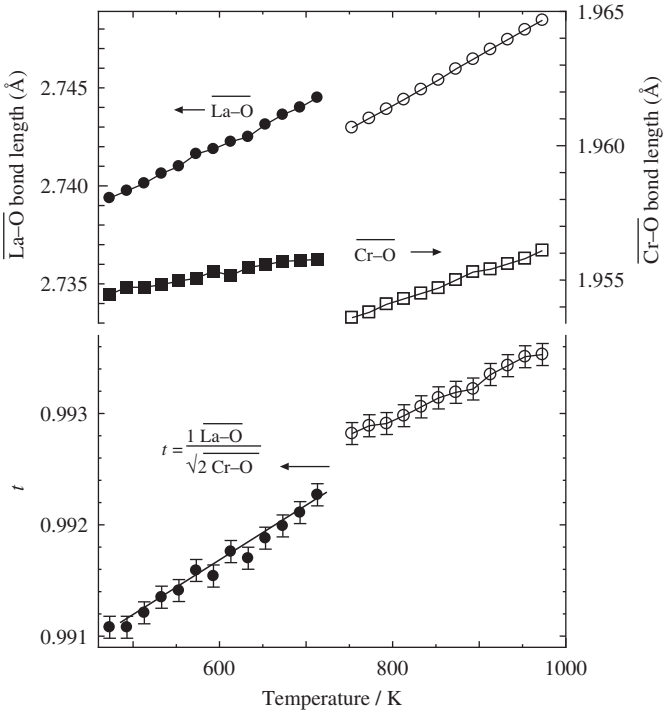

Fig. 13. Temperature dependence of the average bond length of La–O and Cr–O and the parameter, t, of $La_{0.7}Ca_{0.3}CrO_3$.

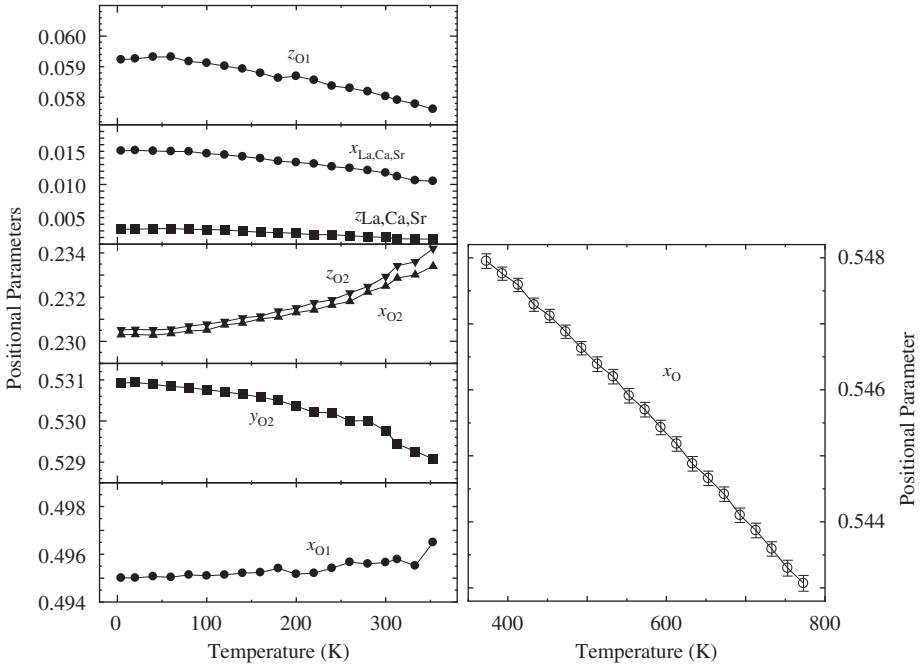

Fig. 12. Temperature dependence of the positional parameters of $La_{0.7}Ca_{0.15}Sr_{0.15}CrO_3$.

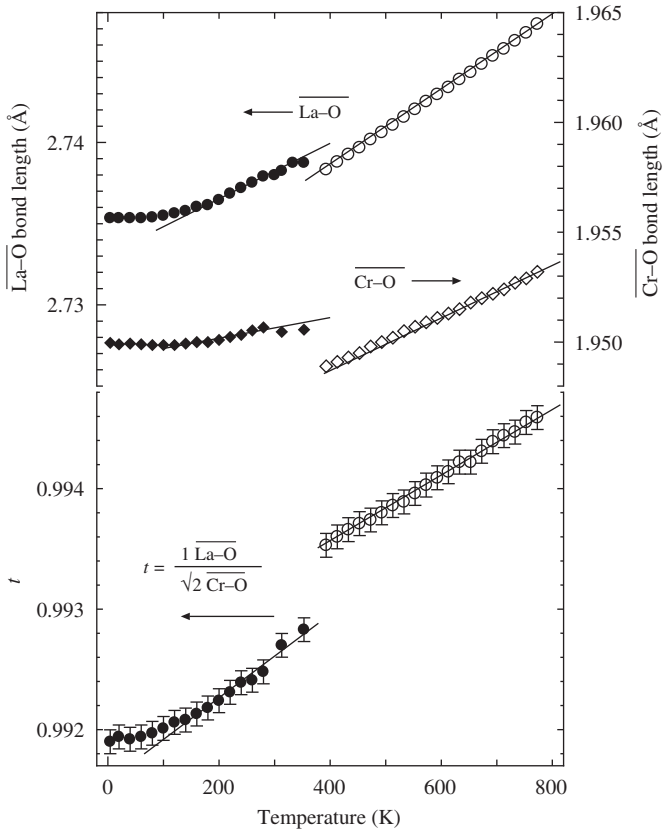

Fig. 14. Temperature dependence of the average bond length of La–O and Cr–O and the parameter, *t*, of $La_{0.7}Ca_{0.15}Sr_{0.15}CrO_3$.

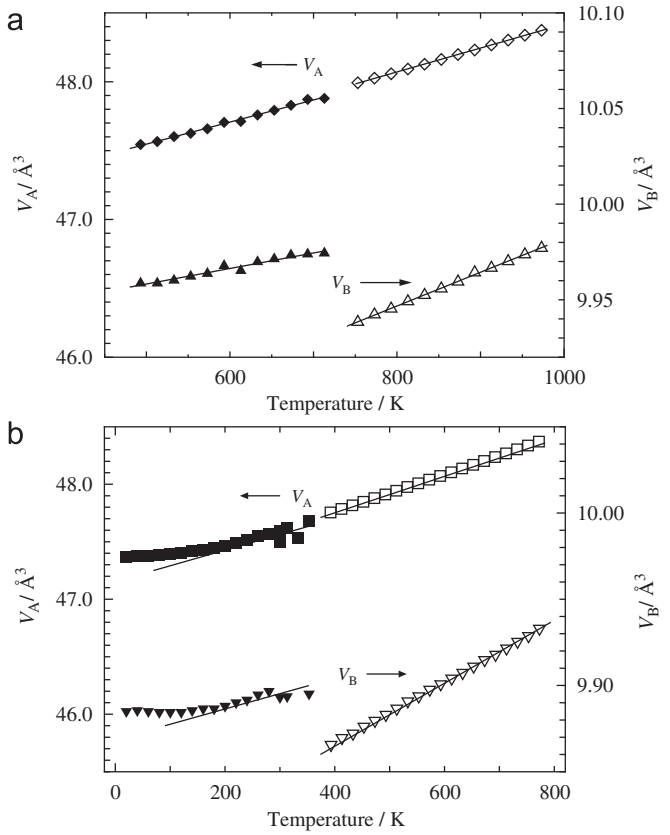

Fig. 15. Temperature dependence of V_A and V_B of (a) $La_{0.7}Ca_{0.3}CrO_3$ and (b) $La_{0.7}Ca_{0.15}Sr_{0.15}CrO_3$.

and V_B within the same phase for both $La_{0.7}Ca_{0.3}CrO_3$ and $La_{0.7}Ca_{0.15}Sr_{0.15}CrO_3$. At the phase transition temperature, only a small change in V_A is observed, whereas a more significant reduction is detected in V_B for both samples, as was also reported in $LaCrO_3$ [22]. Fig. 16 shows the temperature dependence of V_A/V_B and Φ for $La_{0.7}Ca_{0.3}CrO_3$ and $La_{0.7}Ca_{0.15}Sr_{0.15}CrO_3$, which shows similar trends to $LaCrO_3$. V_A/V_B increases and the parameter Φ approaches zero with increase of temperature, indicating that the extent of structural distortion becomes lower at high temperatures. The changes in Φ at the phase transition, $\Delta\Phi$, are 0.0082 and 0.0034 for $La_{0.7}Ca_{0.3}CrO_3$ and $La_{0.7}Ca_{0.15}Sr_{0.15}CrO_3$, respectively. The smaller $\Delta\Phi$ for $La_{0.7}Ca_{0.15}Sr_{0.15}CrO_3$ is attributed to the changes in the positional parameter, *z*, of the cation with temperature within the orthorhombic phase, as shown in Fig. 12. It can be concluded that a smaller $\Delta\Phi$ indicates that the changes in the structural distortion at the phase transition are reduced by Sr substitution. Therefore, it can be expected that a phase transition with smaller $\Delta\Phi$ values shows smaller values of ΔV. As shown in Figs. 9 and 11, a smaller ΔV was observed in $La_{0.7}Ca_{0.15}Sr_{0.15}CrO_3$ than that for $La_{0.7}Ca_{0.3}CrO_3$. Although ΔH cannot be determined purely by geometric differences between the two phases, we suggest that the smaller change in the distortion at the phase transition might simplify the transformation and result in a smaller ΔH, assuming that the geometric transformation enthalpy is predominant. It was reported from DSC measurements that ΔH of 228.9 J/mol for $La_{0.7}Ca_{0.3}CrO_3$ reduced to 120.3 J/mol for $La_{0.7}Ca_{0.15}Sr_{0.15}CrO_3$ [20], supporting the above assumption.

For applications as an interconnecting material within SOFCs, the absence of a structural phase transition is desirable from room temperature to the SOFC operating temperature. Sr substitution is

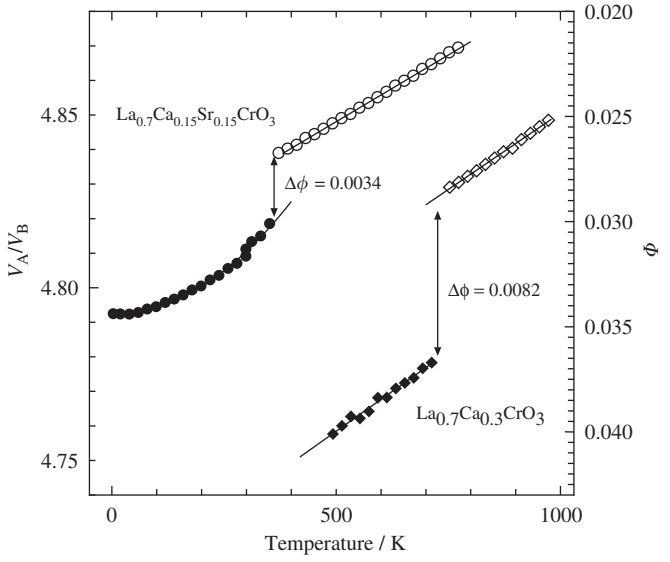

Fig. 16. Temperature dependence of V_A/V_B for $La_{0.7}Ca_{0.3}CrO_3$ (diamonds) and $La_{0.7}Ca_{0.15}Sr_{0.15}CrO_3$ (circles). The parameter, Φ, calculated from V_A/V_B and representing the extent of distortion from the ideal cubic perovskite structure, is shown on the right hand vertical axis.

clearly effective in decreasing the transition temperature within the $La_{0.7}Ca_{0.3-x}Sr_xCrO_3$ system. However, degradation in the sintering properties is observed with larger Sr content. At present, the highest sintering density of more than 95% was observed in the composition $La_{0.7}Ca_{0.15}Sr_{0.15}CrO_3$ [20]. Although the structural

phase transition is observed in $La_{0.7}Ca_{0.15}Sr_{0.15}CrO_3$ between 353 and 373 K, the changes in the structural distortion at the phase transition are small, as Fig. 16 shows, resulting in small values of ΔH and ΔV.

4. Conclusions

Variable temperature neutron powder diffraction measurements have clarified the effects of temperature on the crystal structure of $La_{0.7}Ca_{0.3-x}Sr_xCrO_3$ ceramics. Specifically, the average bond lengths, volumes of the [(La/Sr/Ca)O_{12}] polyhedron and [CrO_6] octahedron have been used to probe the compositional and temperature dependence of Φ, which represents the extent of distortion from the ideal cubic perovskite structure. It is shown that the structural distortions within $La_{0.7}Ca_{0.3-x}Sr_xCrO_3$ become lower with increasing Sr content or temperature. At the structural phase transition from the orthorhombically distorted perovskite arrangement to the rhombohedrally distorted one, a reduction in the size of the [CrO_6] octahedra is observed, whilst the [(La/Sr/Ca)O_{12}] polyhedra show little change. The parameter, $\Delta\Phi$, which represents the difference between the values of Φ between the orthorhombic and rhombohedral phases at the structural phase transition, decreases with increasing Sr content, and consequently shows an agreement with the observed decrease in the enthalpy change, ΔH, and volume change, ΔV, with increasing Sr content. Since $\Delta\Phi$ of $La_{0.7}Ca_{0.15}Sr_{0.15}CrO_3$, which shows the most impressive sintering properties, is smaller than $La_{0.7}Ca_{0.3}CrO_3$, it can be expected that the influence of the phase transition on the mechanical properties of $La_{0.7}Ca_{0.15}Sr_{0.15}CrO_3$ will be smaller. As a consequence, $La_{0.7}Ca_{0.15}Sr_{0.15}CrO_3$ appears to be a promising material for the role of interconnector within future SOFC devices.

Acknowledgments

T. Hashimoto expresses acknowledgement for a grant from the "Strategic Research Base Development" Program for Private Universities subsidized by MEXT (2009) and from Nihon University Strategic Projects for Academic Research "Nanotechnology Excellence—Nanomaterial based Photonic and Quantum Technologies". S. T. Norberg wishes to thank the EU Research and Technology Development Framework Programme for financial support. The UK Science and Technology Facilities Council is thanked for allocating beamtime at the ISIS Facility.

Appendix A. Supplementary material

Supplementary data associated with this article can be found in the online version at doi:10.1016/j.jssc.2009.11.028.

References

[1] N.Q. Minh, J. Amer. Ceram. Soc. 76 (1993) 563.
[2] N.M. Sammes, R. Ratnaraj, J. Mater. Sci. 30 (1995) 4523.
[3] N.M. Sammes, R. Ratnaraj, M.G. Fee, J. Mater. Sci. 29 (1994) 4319.
[4] S.W. Paulik, S. Baskaran, T.R. Armstrong, J. Mater. Sci. 33 (1998) 2397.
[5] N. Sakai, T. Kawada, H. Yokokawa, M. Dokiya, T. Iwata, J. Mater. Sci. 25 (1990) 4531.
[6] S.A. Howard, J. Yan, H.U. Anderson, J. Amer. Ceram. Soc. 75 (1991) 1685.
[7] H.E. Höffer, W.F. Kock, J. Electrochem. Soc. 140 (1993) 2889.
[8] N. Sakai, S. Stølen, J. Chem. Thermodyn. 27 (1995) 493.
[9] T. Hashimoto, K. Takagi, K. Tsuda, M. Tanaka, K. Yoshida, H. Tagawa, M. Dokiya, J. Electrochem. Soc. 147 (2000) 4408.
[10] T. Hashimoto, N. Tsuzuki, A. Kishi, K. Takagi, K. Tsuda, M. Tanaka, K. Oikawa, T. Kamiyama, K. Yoshida, H. Tagawa, M. Dokiya, Solid State Ionics 132 (2000) 181.
[11] K. Momma, F. Izumi, J. Appl. Cryst. 41 (2008) 653.
[12] A.M. Glazer, Acta Crystallogr. B 28 (1972) 3384.
[13] A.M. Glazer, Acta Crystallogr. A 31 (1975) 756.
[14] N. Sakai, J. Chem. Thermodyn. 28 (1996) 421.
[15] N. Sakai, T. Kawada, H. Yokokawa, M. Dokiya, T. Iwata, Solid State Ionics 40/41 (1990) 394.
[16] H. Hayashi, M. Watanabe, M. Ohuchida, H. Inaba, Y. Hiei, T. Yamamto, M. Mori, Solid State Ionics 144 (2001) 301.
[17] K. Tezuka, Y. Hinatsu, A. Nakamura, T. Inami, Y. Shimojo, Y. Morii, J. Solid State Chem. 141 (1998) 404.
[18] F. Nakamura, Y. Matsunaga, N. Ohba, K. Arai, H. Matsubara, H. Takahashi, T. Hashimoto, Thermochim. Acta 435 (2005) 222.
[19] K. Homma, F. Nakamura, N. Ohba, A. Mitsui, T. Hashimoto, J. Ceram. Soc. Jpn. 115 (2007) 81.
[20] A. Mitsui, K. Homma, Y. Kumekawa, F. Nakamura, N. Ohba, Y. Hoshino, T. Hashimoto, J. Electrochem. Soc. 155 (2008) A395.
[21] N. Sakai, H. Fjellvâg, B.C. Hauback, J. Solid State Chem. 121 (1996) 202.
[22] K. Oikawa, T. Kamiyama, T. Hashimoto, Y. Shimojyo, Y. Morii, J. Solid State Chem. 154 (2000) 524.
[23] M.P. Pechini, US Patent, 3 (330) (1967) 697.
[24] S. Hull, R.I. Smith, W.I.F. David, A.C. Hannon, J. Mayers, R. Crywinski, Physica B 180–181 (1992) 1000.
[25] A.C. Larson, R.B. Von Dreele, Los Alamos National Laboratory Report, LAUR 86–748, 1985.
[26] N.W. Thomas, A. Beitollahi, Acta Crystallogr. B 50 (1994) 549.
[27] N.W. Thomas, Acta Crystallogr. B 52 (1996) 16.
[28] N.W. Thomas, Acta Crystallogr. B 52 (1996) 954.
[29] R.D. Shannon, Acta Crystallogr. A 32 (1976) 751.